Leaf-level metabolic changes in response to drought affect daytime CO_2 emission and isoprenoid synthesis

S. Nemiah Ladd[1, 2, *], L. Erik Daber[1,*], Ines Bamberger[1, a], Angelika Kübert[1, b], Jürgen Kreuzwieser[1], Gemma Purser[3, 4], Johannes Ingrisch[1, 5], Jason Deleeuw[6], Joost van Haren[6, 7], Laura K. Meredith[6, 8], Christiane Werner[1]

[1] Ecosystem Physiology, Albert-Ludwigs-University of Freiburg, Georges-Köhler-Allee 053/054, 79110 Freiburg, Germany
[2] Department of Environmental Sciences, University of Basel, Bernoullistrasse 30, 4056 Basel, Switzerland
[3] School of Chemistry, The University of Edinburgh, Joseph Black Building, David Brewster Road, Edinburgh, EH9 3FJ, UK
[4] UK Centre for Ecology & Hydrology, Bush Estate, Penicuik, EH26 0QB, U K
[5] Department of Ecology, University of Innsbruck, Sternwartestrasse 15, 6020 Innsbruck, Austria
[6] Biosphere 2, University of Arizona, 32540 S. Biosphere Rd., Oracle, AZ, 85739, USA
[7] Honors College, University of Arizona, 1101 E. Mabel Street, Tucson, AZ, 85719, USA
[8] School of Natural Resources and the Environment, University of Arizona, Tucson, AZ, USA

*Equal contributions

[a] Current address: Atmospheric Chemistry Group, University of Bayreuth (BayCEER), Dr-Hans-Frisch-Straße 1-3, 95448 Bayreuth, Germany
[b] Current address: Institute for Atmospheric and Earth System Research, University of Helsinki, Pietari Kalmin katu 5, 00014 Helsinki, Finland

Email addresses: n.ladd@unibas.ch, erik.daber@cep.uni-freiburg.de, i.bamberger@mail.de, angelika.kuebert@mail.cep.uni-freiburg.de, juergen.kreuzwieser@ctp.uni-freiburg.de. gepurse25@ceh.ac.uk, Johannes.Ingrisch@uibk.ac.at, jdeleeuw@arizona.edu, jvanhare@arizona.edu, laurameredith@arizona.edu, c.werner@cep.uni-freiburg.de

Abstract

Daytime production of CO_2 in leaves is primarily a byproduct of secondary metabolite synthesis, including the production of volatile organic compounds (VOCs). It remains unclear how the carbon fluxes associated with daytime CO_2 production and VOC emission vary among mature trees, and how they are influenced by drought. We used position-specific ^{13}C-pyruvate labeling to investigate leaf CO_2 and VOC fluxes from four tropical species before and during a controlled drought in an enclosed rainforest. Although daytime CO_2 production was always dominated by non-mitochondrial processes, the relative contribution of CO_2 from mitochondria (i.e., the tricarboxylic acid cycle) tended to increase under drought. The legume tree *Clitoria fairchildiana* had less anabolic CO_2 production than the other species, and was also the only one to allocate detectable amounts of the ^{13}C label to VOCs. In *C. fairchildiana* leaves, our data indicate that intermediates from the mevalonic acid pathway are used to produce the volatile monoterpene trans-β-ocimene, but not isoprene. This suggests that geranyl pyrophosphate is the more important intermediate for crosstalk between cytosolic and plastidic isoprenoid synthesis, not isopentenyl pyrophosphate. This apparent crosstalk declined with drought, and although trans-β-ocimene emissions increased, they were primarily sourced from stored intermediates and not *de novo* synthesis.

Key Words: crosstalk, daytime respiration, drought, isoprenoids, position-specific isotope labeling, tropical plants

Introduction

Carbon is exchanged bidirectionally in leaves during daylight hours. Although active photosynthesis results in net uptake of CO_2 throughout the day, plants release carbon in the form of CO_2 from respiration and metabolic processes (Atkin *et al*., 2000; Sweetlove *et al*., 2013; Tcherkez *et al*., 2017; O'Leary *et al*., 2019) and also as volatile organic compounds (VOCs) (Rasmussen, 1970; Monson and Fall, 1989; Harrison *et al*., 2013). In order to understand how net carbon uptake by plants will change under global warming, it is important to understand how the different processes by which plants release CO_2 and VOCs vary in response to environmental stresses (Niinemets *et al*., 2010; Heskel *et al*., 2013; Schimel *et al*., 2015; Wehr *et al*., 2016), in particular to droughts, which are expected to become more frequent and/or intense for many regions (IPCC, 2021). The net change in carbon uptake by plants under drought will be caused not only due to reduced photosynthesis

(e.g., Reddy *et al*., 2004; Pinheiro and Chavez, 2011), but also to changes in CO_2 production through respiration and other metabolic processes (e.g., Metcalfe *et al*., 2010; Zhao *et al*., 2013).

Overall plant CO_2 emissions are dominated by respiration, the catabolic process in the mitochondria which produces CO_2 for energy gain, and which is down-regulated in the light (Atkin *et al.*, 2000; Tcherkez *et al.*, 2005). However, CO_2 emissions from plants can also be anabolic, as it is released as a byproduct during the synthesis of other molecules (Tcherkez *et al*., 2008; Sweetlove *et al*., 2013; O'Leary *et al*., 2019). These processes serve different functions for the plant, but their regulation is not well understood. Therefore, the relative amounts of CO_2 generated by different processes may change as the need for energy and specific metabolites shifts (Tcherkez *et al*., 2017; O'Leary *et al*., 2019).

One way to distinguish the relative importance of different sources of CO_2 production by plants is through labeling with position-specific ^{13}C-enriched central metabolites, such as glucose or pyruvate (Tcherkez *et al*., 2008; Priault *et al*., 2009; Wegener *et al*., 2010; Jardine *et al*., 2014). This approach is based on the fact that different carbon atoms within an individual molecule will be used for distinct biochemical processes. Therefore, the ^{13}C label from different positions is preferentially allocated into different products depending on the prevailing biochemical pathway (Werner *et al*., 2009; Tcherkez *et al*., 2012; Fasbender *et al*., 2018). For compounds like CO_2 that are released by multiple biochemical pathways, the relative amount of ^{13}C enrichment that occurs following the introduction of different position-specific labels can thus be used to determine the relative importance of different production pathways (Priault *et al*., 2009; Tcherkez *et al*., 2017). Carbon atoms from the C2 and C3 positions of pyruvate are only converted to CO_2 by respiration in the tricarboxylic acid (TCA) cycle (**Figure 1, step 1**) (Tcherkez *et al*., 2005; Priault *et al*., 2009). ^{13}C enrichment of CO_2 following labeling with ^{13}C-2-pyruvate is therefore indicative of TCA cycle activity. Carbon atoms from the C1 position of pyruvate are also released due to TCA cycle activity, as pyruvate is decarboxylated to form acetyl-CoA, which is fed into the TCA cycle (**Figure 1**) (Tcherkez *et al*., 2008; Priault *et al*., 2009). However, numerous anabolic processes also decarboxylate pyruvate. For example, pyruvate-derived acetyl-CoA is also the building block of fatty acids and of isoprenoids produced in the cytosolic mevalonic acid (MVA) pathway (**Figure 1, step 5**) (Schuhr *et al*., 2003). Additionally, carbon from the C1 position is also converted to CO_2 when pyruvate combines with glyceraldehyde 3-phosphate (GA-3-P) to form methylerythritol phosphate (MEP) in the plastidic MEP pathway for isoprenoid synthesis (**Figure 1, step 2**) (Dudareva *et al*., 2004). Together, these processes can

cause ^{13}C enrichment of CO_2 following labeling with $^{13}C1$-pyruvate to be greater than ^{13}C enrichment of CO_2 following labeling with $^{13}C2$-pyruvate during the day, when the TCA cycle is downregulated (Tcherkez et al., 2008; Priault *et al*., 2009). The relative difference in ^{13}C enrichment of CO_2 following labeling with each type of pyruvate is thus broadly indicative of the relative significance of CO_2 production from non-mitochondrial anabolic processes.

Position-specific ^{13}C labeling can also be employed to study the synthesis of various plant metabolites, including VOCs, fatty acids, and sterols (Schwender *et al*., 1996; Lichtenthaler et al., 1997; Schuhr *et al*., 2003; Fasbender *et al*., 2018; Werner *et al*., 2020; Ladd *et al*., 2021). This approach can be particularly helpful for understanding the biosynthesis of both volatile and non-volatile isoprenoids, and for assessing the role of metabolic crosstalk between the MEP and MVA pathways for isoprenoid biosynthesis (**Figure 1, step 4 & 5**) (Schuhr *et al*., 2003; Massé *et al*., 2004; Ladd *et al*., 2021). The maintenance of two parallel pathways for isoprenoid synthesis is unique to higher plants and some algae (Arigoni *et al*., 1997; Hemerlin *et al*., 2003), and it has been suggested that plants use this metabolic redundancy to improve their resistance to environmental stressors via the exchange of isopentenyl pyrophosphate (IPP) or other common precursors across the plastid membrane (Hemerlin *et al*., 2012). The prevalence and importance of crosstalk between the MEP and MVA pathways remains controversial, in part because of a lack of identified transporters that can move IPP across the plastid membrane (Rasulov *et al*., 2018; Souza *et al*., 2018). Recent studies with position-specific ^{13}C-pyruvate labeling demonstrate that this approach can distinguish the transfer of precursor molecules between the two isoprenoid synthesis pathways, and offers an opportunity to assess if these rates change with environmental stressors such as heat stress and drought (Werner *et al*., 2020; Ladd *et al*., 2021).

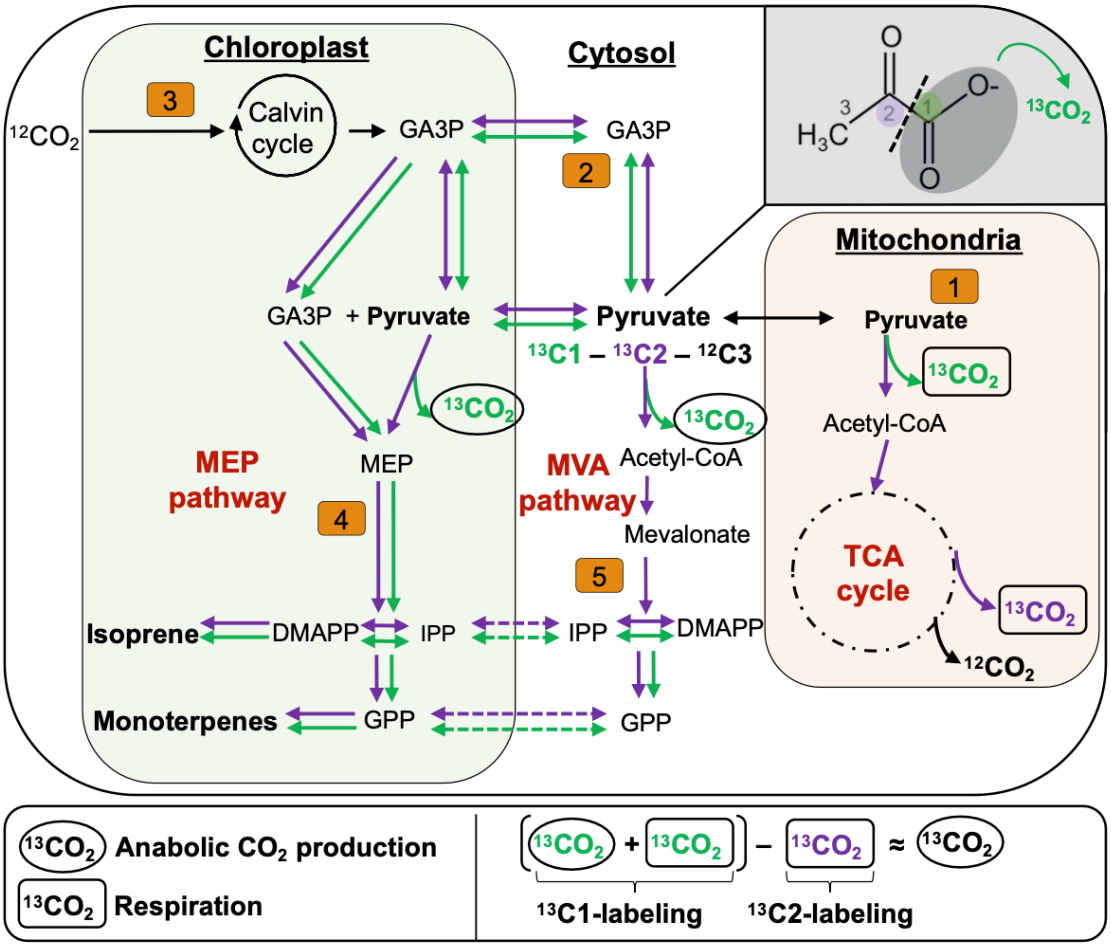

Figure 1: Schematic representation of important processes for the synthesis of isoprenoids and production of CO_2 within plant cells, with several intermediate steps removed for clarity. Green arrows represent possible movement of carbon from the C1 position of pyruvate and purple arrows represent movement of carbon from the C2 position of pyruvate. Numbers represent the relevant pathways discussed. 1: Transport of pyruvate into mitochondria, followed by initial decarboxylation of the C1-position and entrance into the TCA-cycle. 2: Conversion of pyruvate to GA-3-P and transport into the chloroplast. Pyruvate might also be transported directly to the chloroplast. All carbon positions of pyruvate remain in both cases. 3: Entrance of CO_2 into the Calvin cycle and addition of GA-3-P and other assimilation products into the metabolic pool of the chloroplast. 4: Initial reaction of pyruvate and GA-3-P to form DMAPP and IPP via MEP pathway, followed by reaction of two DMAPP/IPP molecules to produce GPP. As GA-3-P is not decarboxylated in this reaction, all carbon positions of the converted GA-3-P remain in the produced isoprene and monoterpenes. Pyruvate on the other hand is decarboxylated, resulting in only the C2-position remaining in these products 5: Entrance of pyruvate into MVA pathway and initial decarboxylation of the C1-position of pyruvate to form DMAPP, IPP and subsequently GPP in the cytosol. After transport of these metabolites incorporating the $^{13}C2$-label into the chloroplast, DMAPP and IPP can either enter isoprene or monoterpene synthesis, while GPP is utilized to synthesize monoterpenes. TCA, tricarboxlic acid; GA-3-P, glyceraldehyde 3-phosphate; DMAPP Dimethylallyl pyrophosphate; IPP, isopentenyl pyrophosphate; MEP, methylerythritol phosphate; GPP, geranyl pyrophosphate; MVA, mevalonic acid.

Previous studies that used position-specific ^{13}C labeling to learn about the production of CO_2 and isoprenoids were conducted under controlled conditions in growth chambers (e.g., Tcherkez *et al*., 2005; Priault *et al*., 2009; Ghirado *et al*., 2014; Jardine *et al*., 2014;

Werner *et al*., 2020; Ladd *et al*., 2021). These growth chamber studies have, by necessity, focused on relatively young and immature plants, and it has remained challenging to conduct a controlled experiment of this type with mature trees integrated within an ecosystem. However, there is also a need to understand how CO_2 and VOC production varies among mature plants in an ecosystem context, as this is more representative of how such fluxes respond to environmental change in nature (Guenther *et al*., 1995; Peñuelas and Staudt, 2010; Materić *et al*., 2015). Additionally, most growth chamber studies have focused on temperate plants, meaning that little is known about these dynamics in tropical forests, despite the potential risk that they will change from carbon sinks to sources due to climate change (Mitchard 2018; Hubau et al., 2020), further affecting their VOC emissions (Peñuelas and Llusià 2003)

To assess the metabolic processes responsible for daytime emissions of CO_2 and volatile isoprenoids in mature plants, and to determine if these carbon fluxes change with drought stress, we used position-specific ^{13}C-pyruvate labeling to study leaf level CO_2 and VOC fluxes before and during drought in an enclosed rainforest at the Biosphere 2 research facility, as part of the Biosphere 2 Water Atmosphere and Life Dynamics (B2WALD) campaign. We focused on fluxes from four tropical plant species, including two canopy forming trees (*Clitoria fairchildiana* and *Phytolacca dioica*) and two understory plants (*Hibiscus rosa sinensis* and *Piper auritum*), representing a range of functional responses to drought (Werner *et al*., 2021). We calculated the amount of pyruvate label from both the C1 and the C2 position that was allocated to CO_2 and, in the case of *C. fairchildiana*, to emissions of isoprene and monoterpenes to gain insights into possible metabolic adjustments towards drought.

Materials and Methods

Drought campaign

This study took place within the context of the broader B2WALD campaign, described in detail by Werner *et al*. (2021). The B2WALD campaign made use of the unique thirty-year-old enclosed rainforest at the Biosphere 2 research facility, located north of Tucson, AZ, USA. In 2019, this manipulatable, mature ecosystem was subjected to a 65-day drought, with intensive monitoring of gas fluxes from leaves, stems, soils, and roots throughout a 110-day period before, during, and after drought (Werner *et al*., 2021). Under non-drought conditions, the Biosphere 2 rainforest receives 1600 mm/year, distributed by overhead sprinklers three times per week. Following the rain event on the night of 7 October

2019, we turned off the sprinkler system and did not add additional water to the system until 2 December 2019 (Werner *et al*., 2021). Daytime temperatures within the canopy of the Biosphere 2 rainforest ranged from 23.3 to 33.5 °C during the pre-drought period and 22.2 to 34.8 °C during the drought. Corresponding daytime temperature ranges for the understory were 21.3 - 26.6 °C and 22.2 - 29.6, respectively. While there were no seasonal trends in the temperature inside the biome, maximum PAR values outside the enclosure declined from 1685 to 1016 μmol m^{-2} s^{-1} (Werner *et al*., 2021).

During the first four weeks of drought in the Biosphere 2 rainforest, surface soil moisture was almost completely depleted and the atmospheric vapor pressure deficit increased in both the canopy and the understory, but at a higher rate in the canopy (Werner *et al*., 2021). In normal years there is no seasonal variability in precipitation within the Biosphere 2 rainforest, and the ecosystem scale changes in water and carbon fluxes differed significantly from seasonal changes associated with reduced external light availability (Werner *et al*., 2021). Changes in water fluxes by individual plants were also clearly driven primarily by drought and not light availability, as the trees' sap flow increased immediately when rain first returned to the system in mid-December (Werner *et al.*, 2021), when ambient light levels are at their annual minimum.

Plant species selection

For this study, we focused on leaf fluxes from four species in the Biosphere 2 rainforest, which were among the most abundant taxa in the forest and were selected to represent a range of drought responses and microclimates within the forest. *Clitoria fairchildiana* R.A. Howard, a large, canopy forming tree, makes up ~30 % of the forest canopy. *Phytolacca dioica* L. also represents another large canopy forming tree, and we included two large individuals as well as two smaller individuals. From the understory, we included the fast-growing, herbaceous perennial from the genus *Piper*, most likely *Piper auritum* Kunth, and *Hibiscus rosa sinensis* L., an evergreen woody shrub.

Gas sampling system and analyzers

For all target species, we enclosed whole leaves in species-specific, flow-through ventilated cuvettes made from FEP film and PFA tubing as in Fasbender *et al.* (2018). One end of the leaf cuvette was sealed around the petiole, while the other end was sealed around the incoming and outcoming PFA tubes. For *H. rosa sinensis*, we used larger cuvettes that enclosed several leaves on terminal branches. This was necessary because it was difficult to

avoid embolism when cutting the petiole of single *H. rosa sinensis* leaves. We equipped each cuvette with a data logger and a light sensor that recorded light levels at an angle parallel to the leaf's surface, as well as thermocouple that recorded leaf surface temperatures. Leaf temperatures inside the leaf cuvettes did not exceed daytime ecosystem temperature maxima reported in Werner et al. (2021) (**Table S1**).

We continuously supplied each cuvette with a mix of VOC and CO_2-free air produced by a Zero Air Generator (Aadco Instruments, Inc., Cleves, OH, USA) and a constant amount of CO_2 (~500 ppm, $\delta^{13}C$ ~ -10 ‰) from a gas tank. Each cuvette was equipped with a fan to guarantee efficient air mixing. The outflow from the cuvette was connected to a Teflon T-piece and ball valve that allowed us to sample a portion of the flow onto cartridges for offline analyses (details below). Additional flow was diverted to three analyzers: (1) a proton transfer reaction – time of flight mass spectrometer (PTR-TOF-MS 4000ultra, Ionicon Analytic, Innsbruck, Austria) for VOC fluxes, (2) a carbon isotope laser spectrometer (Delta Ray IRIS, Thermo Fisher Scientific, Bremen, Germany) for concentrations and stable isotopes of CO_2, and (3) a water isotope cavity ring-down spectrometer (L2120i water isotope analyzer, Picarro Inc., Santa Clara, CA, USA) concentrations and stable isotopes of water vapor. Details of the gas sampling system, analyzers, and the calibration of different analyzers used during the B2WALD campaign are provided in Werner *et al*. (2021).

Position-specific ^{13}C-pyruvate labeling

We conducted position-specific ^{13}C-pyruvate labeling during two time periods: pre-drought (12 – 28 September 2019) and drought (4 – 16 November, 2019; after 27 – 39 days without rain), using a protocol similar to that of Fasbender *et al*. (2018). For canopy trees, we did the labeling during the morning hours, when overall photosynthesis tends to be highest in the Biosphere 2 rainforest, as hot temperatures in the sunlit canopy induce early stomatal closures (Rascher *et al*., 2004; Rosolem *et al*., 2010). For the cooler understory, we did most of the labeling in the afternoon. Leaves were installed in cuvettes at least one day prior to the labeling event. Immediately prior to labeling, we monitored the cuvette for 15 minutes to ensure that leaf fluxes were stable. We then cut the leaf petiole and rapidly placed it under water, and cut it again to avoid embolism. The petiole remained in an Eppendorf tube filled with water for five more minutes so that the fluxes could stabilize after cutting. Subsequently, we exchanged the Eppendorf tube with one containing a 10 mM solution of either $^{13}C1$- or $^{13}C2$-pyruvate (99 atom % ^{13}C, Cambridge Isotope Laboratories, Andover, MA, USA). We

used the change in mass of the Eppendorf tube relative to the pre-measurement mass to calculate the mass of label uptake.

We collected the leaf after each measurement to determine its leaf area by tracing it on a sheet of paper of known mass and weighing the leaf's shape on a fine mass-balance. We filled missing leaf area values with the median value of all leaves of the same species (n = 16).

Cartridge sampling and analyses

During each pyruvate labeling event, we also collected VOCs on glass cartridges filled with 50 mg of Tenax. We used an air sampling pump (220-1000TC, SKC, Eighty Four, PA, USA) to maintain a defined air flow (100 - 200 ml min^{-1}) through the cartridge. We attached the cartridges to the cuvette for at least 30 minutes prior to the leaf cutting and for ~70 minutes while the leaf petiole was submersed in the pyruvate solution. Parallel to the collection of each cartridge from the leaf cuvette, we collected a cartridge from an empty cuvette to correct for cuvette background and potential contaminants. After sample collection we sealed the cartridges in vacutainers and stored them at room temperature prior to analysis.

We subsequently analyzed all cartridge samples by Gas Chromatography – Mass Spectrometry – Combustion interface – Isotope Ratio Mass Spectrometry (GC-MS – C – IRMS) at the University of Freiburg to identify and quantify the emitted VOCs and to determine the $\delta^{13}C$ values of individual VOCs. Volatiles were analyzed after thermodesorption on a gas GC (7890B, Agilent Technologies Böblingen, Germany) equipped with a mass-selective detector (MSD, 5975C, Agilent Technologies Böblingen, Germany) and a thermodesorption/cold injection system (TDU-CIS4, Gerstel, Germany). VOCs were desorbed from cartridges at 220 °C and immediately trapped in the CIS at −70°C. The CIS was heated up to 240 °C, channeling the volatiles onto the separation column (DB-5ms UI, 30 m × 0.25 mm ID, 0.25 µm film thickness, Agilent Technologies Böblingen, Germany). Further details on GC oven and MSD settings are given by Haberstroh *et al*. (2018). To quantify specific compounds (i.e., main monoterpenes including trans-β-ocimene), we regularly analyzed calibration curves with authentic standards. We analyzed chromatographic raw data with MassHunter Software (Agilent Technologies Böblingen, Germany). We compared mass spectra with the NIST mass spectral library and the retention times of authentic standards to identify compounds of interest.

10 % of the column effluent was diverted to the MSD by a splitter at the end of the GC column, while the remainder of the sample was transferred to an Isotope Ratio Mass Spectrometer (IRMS; Isoprime precisION, Elementar, Hanau, Germany) via a combustion furnace (GC5 interface, Elementar, Hanau, Germany). The latter was operated at 850 °C and combusted VOCs with CuO to CO_2 and water. After removal of water by a Nafion trap, the CO_2 was directed into the continuous flow IRMS to analyze compound specific $\delta^{13}C$ values. We regularly analyzed octane ($\delta^{13}C$: −31.75 ± 0.01 ‰) and octadecane ($\delta^{13}C$: −32.70 ± 0.01 ‰) (available from Schimmelmann lab, Indiana University, https://arndt.schimmelmann.us/compounds.html) as isotopic reference standards throughout the measurement window. We analyzed raw data with the IonIOS software (Elementar Analysensysteme GmbH, Langenselbold, Germany).

Calculations

For all calculations, we used 15-minute averages from the end of the labeling period (minute 55-70 after label application) in order to minimize the effects of any disturbance from cutting the leaf and placing it into solution. We calculated the transpiration rate E [mmol $m^{-2}s^{-1}$] and the assimilation rate A [µmol $m^{-2}s^{-1}$] from the concentration of water vapor and CO_2 as in von Caemmerer and Farquahar (1981), using the concentrations from the stable isotope spectrometers (Picarro L2120i and Thermo Delta Ray, respectively). We calculated instantaneous water use efficiency WUE_i [µmol CO_2/mmol H_2O] as the ratio A/E.

The Delta Ray calculated $\delta^{13}C$ values of CO_2 relative to the Vienna Pee Dee Belemenite (VPDB) scale using two internal reference gases ($\delta^{13}C$ values = -9.86 ‰ and -27.8 ‰). We calculated the ^{13}C enrichment of CO_2 ($\varepsilon^{13}C_{CO2}$) leaving the leaf cuvettes following labeling with ^{13}C-pyruvate as

$$\varepsilon^{13}C_{CO2} = \left(\frac{\delta^{13}C_{CO2o} + 1000}{\delta^{13}C_{CO2e} + 1000} - 1\right) \quad (1)$$

where $\delta^{13}C_{CO2o}$ and $\delta^{13}C_{CO2e}$ are the $\delta^{13}C$ values of CO_2 from the outlet and the entrance of the cuvette, respectively. The term $\varepsilon^{13}C_{CO2}$ is functionally equivalent to $\Delta^{13}C_{CO2}$ as it is frequently used in plant sciences.

We converted $\delta^{13}C$ values to the fraction of ^{13}C ($^{13}F = {}^{13}C/({}^{12}C + {}^{13}C)$) using the definition of $\delta^{13}C$ and the known $^{12}C/^{13}C$ ratio of VPDB (Hayes, 2004). We then used isotopic mass balance to determine the net isotopic effect of photosynthesis and respiration on the ^{13}F value of CO_2 leaving the leaf cuvette, $^{13}F_{CO2}$, prior to labeling as:

$$^{13}F_P = \frac{c_e * {}^{13}F_e - c_o * {}^{13}F_o}{c_e - c_o} \quad (2)$$

Where $^{13}F_e$ and $^{13}F_o$ are the ^{13}F values for CO_2 and c_e and c_o are the concentrations of CO_2 at the entrance and outlet of the leaf cuvette, respectively. We averaged $^{13}F_P$ values for all measurements of each species, and assumed that it remained constant throughout the pyruvate labeling event, because the natural isotope effect of photosynthesis and respiration on the δ^{13}C value of the CO_2 leaving the cuvette was relatively small (always less than 10 ‰) relative to the impact of the ^{13}C pyruvate label.

We were then able to calculate the concentration of ^{13}C originating from the pyruvate label, c_l, through isotopic mass balance as:

$$c_I = \frac{c_o * (F_o - F_P) + c_e * (F_P - F_e)}{F_I} \quad (3)$$

where the ^{13}F value of the 99 atom % ^{13}C-pyruvate label, F_l, is 0.99. We converted c_l to moles of CO_2 using the ideal gas law and the flow rate of air to the leaf cuvettes, and to grams of CO_2 using the molar mass of CO_2. We then compared this mass to the total mass of ^{13}C taken up from the pyruvate label to determine the percent of pyruvate carbon that was allocated to CO_2.

VOC fluxes V_l in [*nmol* $m^{-2}s^{-1}$] were calculated from molar flow, the leaf area, the concentration of the VOC from the outlet of the empty cuvette v_e [*ppb*], and the concentration of the VOC at the outlet of the leaf cuvette v_o [*ppb*] as:

$$V_l = \frac{u}{s} * (v_o - v_e) \quad (4)$$

To distinguish VOCs that were synthesized directly from introduced ^{13}C1- or ^{13}C2-pyruvate, $^{13}V_l$, and VOCs produced only with ^{12}C, $^{12}V_l$, we calculated the fraction of the fluxes of mass 69.0683 in relation to mass 70.0719 for isoprene and mass 137.141 in relation to mass 138.145 for monoterpenes. We subsequently subtracted the theoretical value of the contribution of the heavier isotope under natural abundance of ^{13}C (1.1%), $^{13}F_{na}$ (isoprene: 5.5%; monoterpenes: 11%) to calculate the excess ^{13}C fraction $^{13}F_{Vl}$ in percent:

$$^{13}F_{Vl} = \frac{^{13}V_l}{^{13}V_l + {}^{12}V_l} * 100 - {}^{13}F_{na} \quad (5)$$

To calculate ^{13}C enrichment of individual monoterpenes measured by GC-C-IRMS, we calculated ε^{13}C values between the δ^{13}C value of the compound during a specific labeling

event ($\delta^{13}C_l$) and the mean $\delta^{13}C$ value of the same compound from unlabeled leaves ($\delta^{13}C_n$) during the same experimental phase (pre-drought or drought):

$$\varepsilon^{13}C = \left(\frac{\delta^{13}C_l+1000}{\delta^{13}C_n+1000} - 1\right) \quad (6)$$

Statistics

Changes in transpiration, assimilation, leaf water potential, VOC fluxes, and ^{13}C-enrichment of CO_2 between pre-drought and drought measurements were compared for each species using Welch's t test. Differences in ^{13}C-enrichment of CO_2 were also assessed using three-way ANOVA followed by Tukey's post hoc test, with species, drought treatment, and position of ^{13}C in the pyruvate label as separate factors. All statistical analyses were performed in GraphPad Prism software.

Results

Changes in transpiration, assimilation, and leaf water use efficiency

Transpiration and assimilation rates declined during the drought for all species besides *H. rosa sinensis*, which had low rates in both periods (**Figure 2**). *P. dioca* displayed the highest intraspecies variability in these fluxes, with very high values observed for the leaves of the largest individual, located on the south side of the biosphere, which received more direct sunlight than the trees on the north side. *C. fairchildiana* displayed the largest relative reductions in transpiration and assimilation, with a relatively greater decline in assimilation, resulting in a significant decrease in water use efficiency (WUE) during the drought (**Figure 2**). Nevertheless, *C. fairchildiana* had the highest WUE of any species in both phases of the experiment (**Figure 2**).

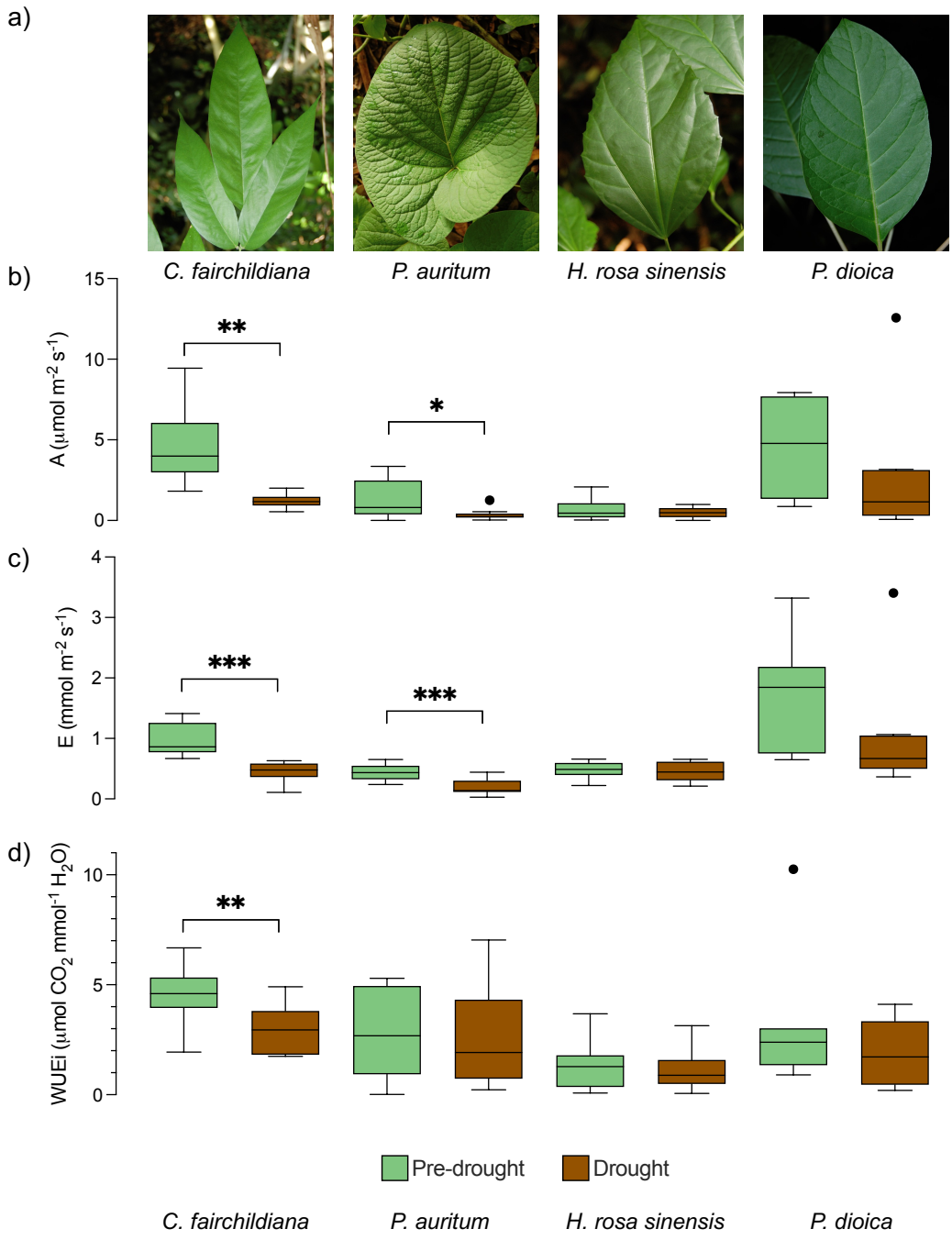

Figure 2: Representative leaves (panel a) and rates of (b) carbon assimilation, (c) transpiration, and (d) instantaneous water use efficiency measured on individual leaves of *Clitoria fairchildiana*, *Piper auritum, Hibiscus rosa sinensis*, and *Phytolacca dioica* under pre-drought (green) and drought (brown) conditions. Boxes represent the median and 25 – 75 % range of 7-12 replicate leaves. Whiskers and outliers calculated using Tukey's method. Significant differences between pre-drought and drought conditions for each species are indicated as * when $p < 0.05$, ** when $p < 0.01$, and *** when $p < 0.001$.

VOC fluxes

C. fairchildiana had the highest isoprene fluxes of all species under both pre-drought (7 ± 3 nmol m^{-2} s^{-1}) and drought (1.1 ± 0.9 nmol m^{-2} s^{-1}) conditions (**Figure 3**). *P. auritum* had the second highest isoprene fluxes, but these were an order of magnitude lower than those from *C. fairchildiana* (0.1 ± 0.04 nmol m^{-2} s^{-1} under pre-drought conditions and $1*10^{-4} \pm 9*10^{-5}$ nmol m^{-2} s^{-1} under drought conditions; **Figure 3**). Isoprene emissions from *H. rosa sinensis* and *P. dioica* were another one to two orders of magnitude lower than those from *P. auritum*. Between the pre-drought and drought, isoprene emissions only declined significantly for *P. auritum* ($p < 0.05$), but there were declining tendencies in emissions for *C. fairchildiana* and *P. dioica* as well (**Figure 3**).

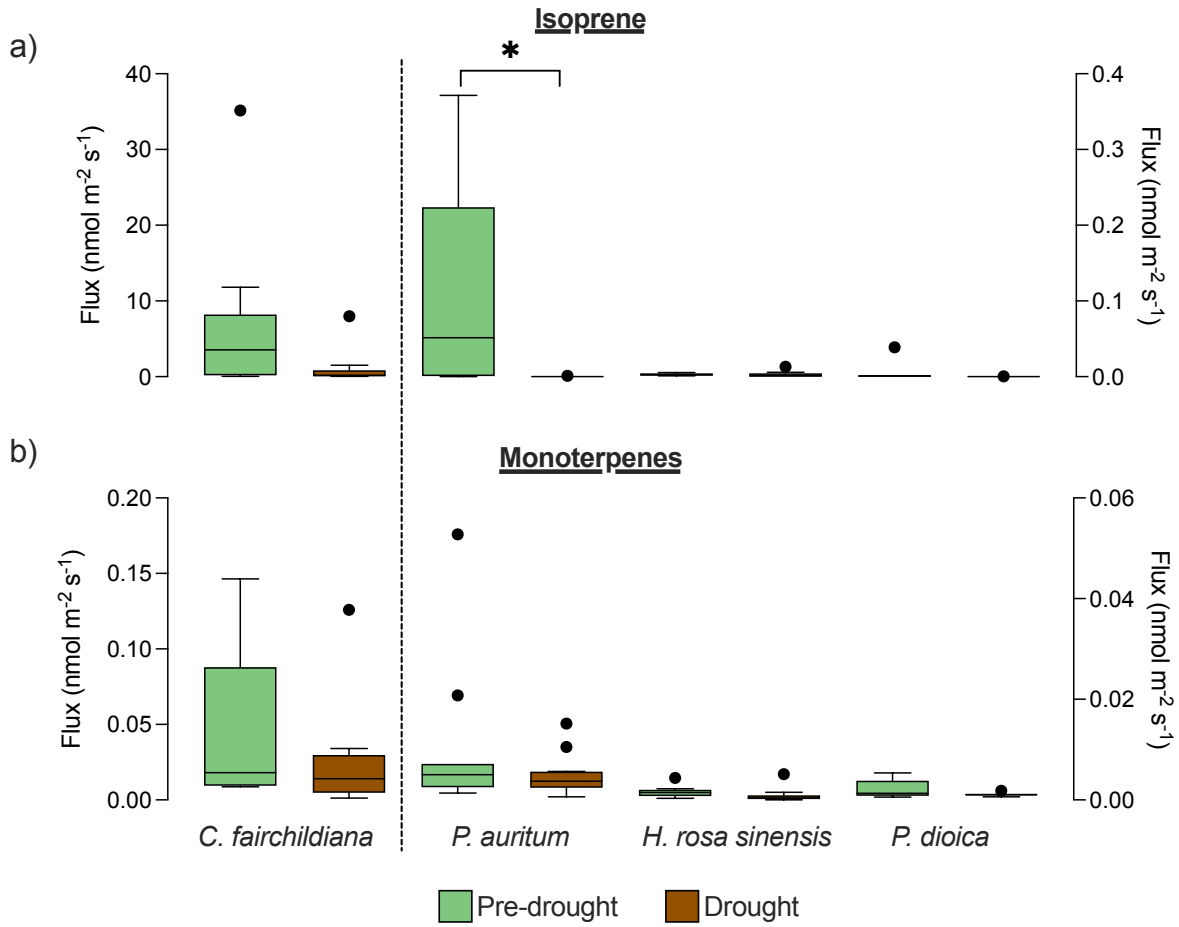

Figure 3: Emission rates of (a) isoprene and (b) monoterpenes measured on individual leaves of *Clitoria fairchildiana*, *Piper auritum, Hibiscus rosa sinensis*, and *Phytolacca dioica* under pre-drought (green) and drought (brown) conditions. Fluxes from *C. fairchildiana* are plotted on the left y-axis while all other species are plotted on the right y-axis. Boxes represent the median and 25 – 75 % range of 7-12 replicate leaves. Whiskers and outliers are calculated using Tukey's method. Significant differences between pre-drought and drought conditions for each species are indicated as: * when $p < 0.05$.

Monoterpene emissions were also at least an order of magnitude higher from *C. fairchildiana* than any other species (**Figure 3**), but were two orders of magnitude lower than its isoprene emissions. Monoterpene emissions declined for all species under drought (**Figure 3**), but not significantly. Analysis of cartridge samples by GC-MS (which is able to chromatographically resolve different monoterpenes) indicated that α-pinene, β-pinene, 3-carene, limonene, and trans-β-ocimene were the most abundant monoterpenes emitted by *C. fairchildiana* (**Table 1**). Fluxes of most of these compounds declined with drought, but trans-β-ocimene emissions increased by a factor of four (**Table 1**).

Table 1: Fluxes of common monoterpenes emitted by *Clitoria fairchildiana*, as determined by GC-MS analysis. Monoterpene fluxes from the other three species were too low for quantification by GC-MS. Fluxes are reported as mean and standard error. [1]These two compounds co-eluted on the GC and the combined flux is reported.

	Pre-drought flux (pmol m^{-2} s^{-1})		Drought flux (pmol m^{-2} s^{-1})		Significant change with drought
α-pinene	6.51	± 2.41	3.09	± 0.20	$p < 0.001$
d-3-carene/ β-pinene[1]	9.28	± 2.96	5.52	± 0.46	$p < 0.01$
limonene	5.10	± 0.79	4.39	± 0.23	$p < 0.05$
trans-β-ocimene	5.47	± 1.20	28.88	± 7.35	$p < 0.0001$

^{13}C-enrichment of CO_2 from pyruvate

All studied plants in Biosphere 2 displayed the expected pattern of more ^{13}C-enriched CO_2 following labeling with $^{13}C1$-pyruvate than with $^{13}C2$-pyruvate (**Figures 4, 5**). The difference in the percentage of ^{13}C from pyruvate that was converted to CO_2 was highly significant for most species during pre-drought, but was not significantly different for *C. fairchildiana* at any time, nor for *P. auritum* during drought (**Figure 4**). As much as ~10 % of the total ^{13}C from the $^{13}C1$-pyruvate was respired during the relatively short period of our measurement, in contrast to less than 1.5 % of the total ^{13}C taken up from the $^{13}C2$-pyruvate (**Figure 4**). However, the magnitude of this difference tended to be less pronounced for *C. fairchildiana* and *P. auritum* than for *H. rosa sinensis* and *P. dioica* (**Figures 4, 5)**. This difference is apparent by plotting the $\varepsilon^{13}C_{CO2}$ (i.e., the change in $\delta^{13}C$ values of CO_2 due to labeling) values from $^{13}C1$-pyruvate labeling relative to those from $^{13}C2$-pyruvate labeling, where the values for *C. fairchildiana* and *P. auritum* plot much closer to the 1:1 line than the

other species do (**Figure 5**). During drought, the $\varepsilon^{13}C_{CO2}$ values during labeling with both pyruvate labels tended to decline for both *C. fairchildiana* and *P. auritum*, while for *P. dioica* they only tended to decline for labeling with ^{13}C1-pyruvate and for *H. rosa sinensis* they did not change (**Figure 5**).

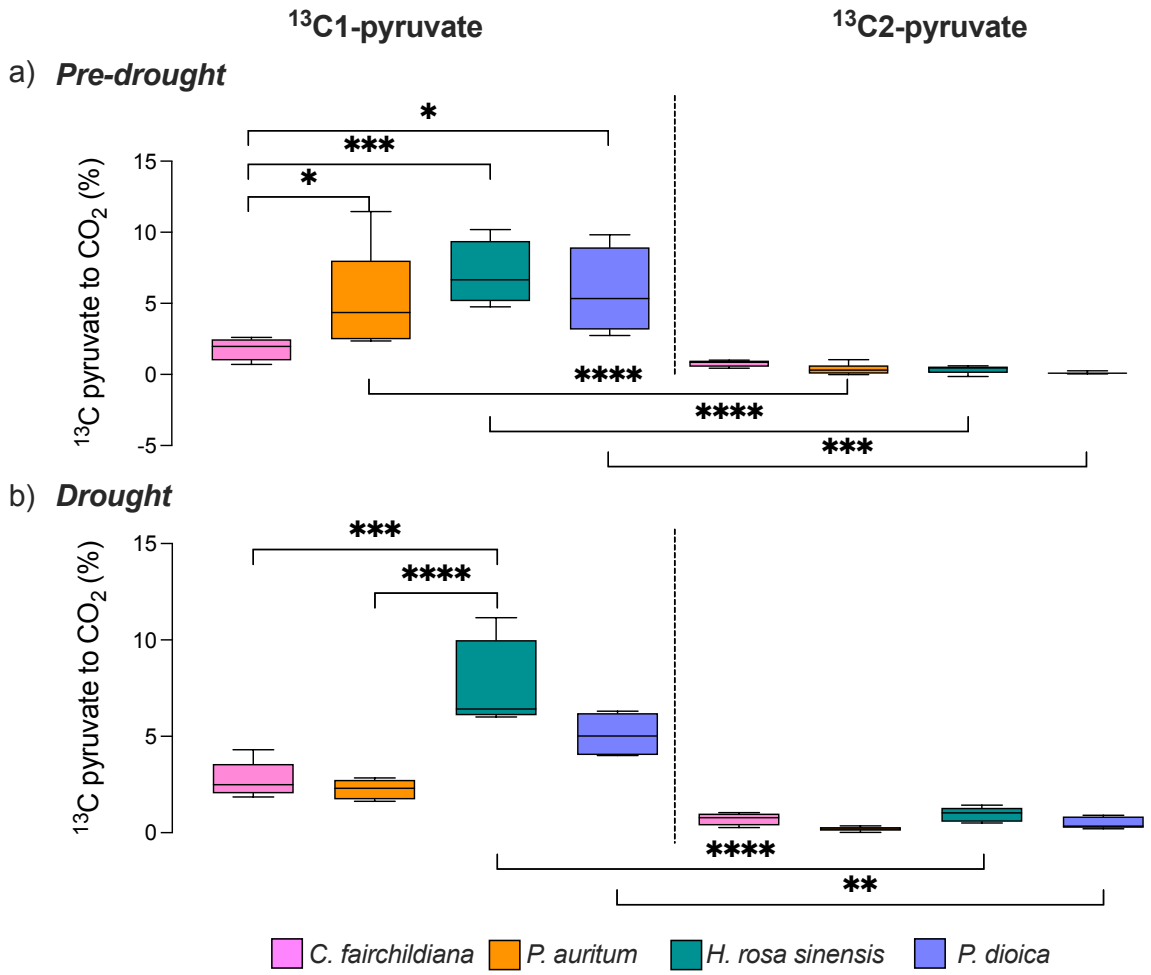

Figure 4 Percent of ^{13}C from ^{13}C1-labeled pyruvate (left column) and ^{13}C2-labeled pyruvate (right column) that was released as CO_2 by *Clitoria fairchildiana*, *Piper auritum, Hibiscus rosa sinensis*, and *Phytolacca dioica* under pre-drought (panel a) and drought (panel b) conditions. Boxes represent the median and 25 – 75 % range of 3 - 6 replicate leaves. Whiskers and outliers are calculated using Tukey's method. Significant differences among groups as determined by three-way ANOVA with Tukey's posthoc test are indicated as: * when $p < 0.05$, ** when $p < 0.01$, *** when $p < 0.001$, and **** when $p < 0.0001$.

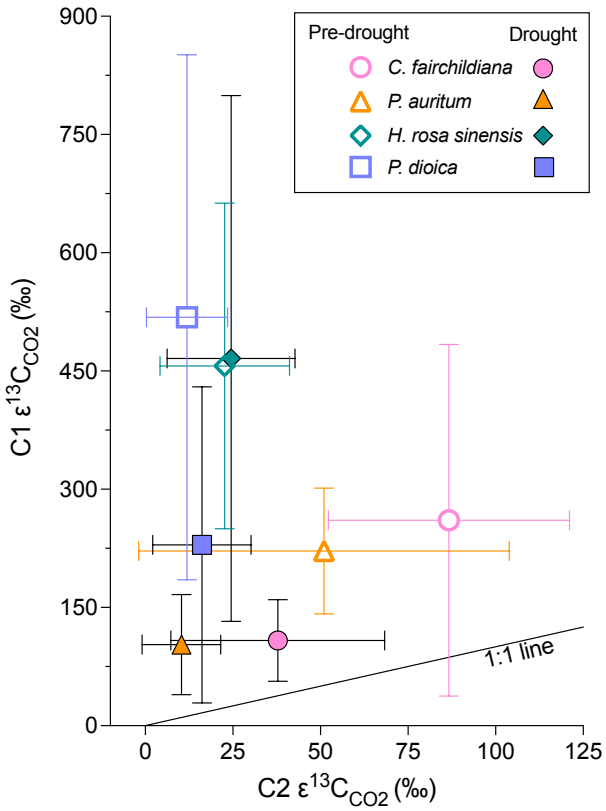

Figure 5 ^{13}C enrichment of CO_2 from $^{13}C1$-labeled pyruvate (y-axis) plotted relative to ^{13}C enrichment of CO_2 from $^{13}C2$-labeled pyruvate (x-axis) during pre-drought (open symbols) and drought (closed symbols). Symbols represent mean values and error bars represent one standard deviation of 3 – 6 replicate leaves per species.

^{13}C-enrichment of VOCs following pyruvate labeling

Emissions of isoprene and monoterpenes in *C. fairchildiana* were clearly enriched in ^{13}C following the ^{13}C-pyruvate labeling during both pre-drought and drought conditions. For isoprene, up to 15 % of the isoprene flux was labeled with ^{13}C above the natural background level (**Figure 6a**), indicating that a sizable amount of isoprene was freshly synthesized from pyruvate. During pre-drought conditions, there was no significant difference in the incorporation of ^{13}C into isoprene fluxes from the $^{13}C1$- and $^{13}C2$-pyruvate labels (**Figure 6a**). Similarly, under drought, there was no significant difference in ^{13}C-incorporation between both labels. However, ^{13}C-incorporation in isoprene increased under drought, though this was significant only for $^{13}C1$-labeling (**Figure 6a**).

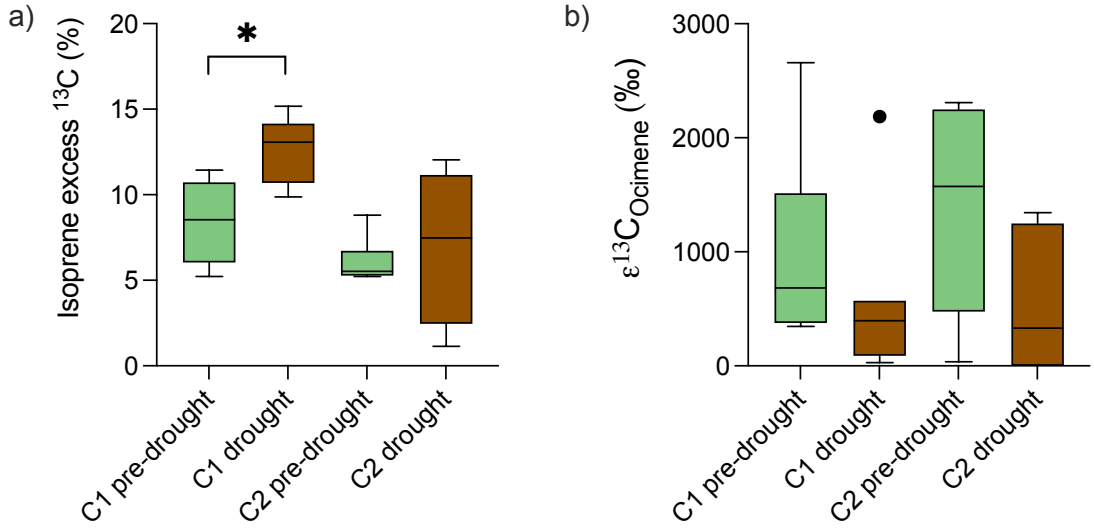

Figure 6: ^{13}C from ^{13}C-labeled pyruvate incorporation into VOCs from *Clitoria fairchildiana*. (a) ^{13}C excess isoprene emissions relative to natural background ^{13}C abundance for isoprene and (b) ^{13}C enrichment of the monoterpene trans-β-ocimene relative to unlabeled measurements during pre-drought (green) and drought (brown) (4 – 6 replicates per treatment). Boxes represent median and 25-75% range of 7-12 replicate leaves. Whiskers and outliers are calculated using Tukey's method.

Of the monoterpenes emitted from *C. fairchildiana*, only trans-β-ocimene was strongly enriched in ^{13}C following labeling by either type of pyruvate, with relatively higher ^{13}C enrichment from $^{13}C2$-pyruvate than from $^{13}C1$ (**Figure 6b**). Under drought, trans-β-ocimene ^{13}C enrichment was similar from both pyruvate labels, with a tendency to decline under drought (**Figure 6b**).

Discussion

We used position specific ^{13}C-pyruvate labeling to investigate leaf level metabolic processes before and during an experimental drought in the Biosphere 2 tropical rainforest, with an emphasis on understanding sources of daytime CO_2 production and isoprenoid synthesis. We focused on four tropical species with clear differences in their drought responses (**Figure 7**). Our results demonstrate that the relative contribution of processes driving daytime CO_2-production is species-specific and can shift due to environmental stressors, such as drought. Although anabolic processes are expected to dominate total daytime CO_2-production, this distinction was muted in the nitrogen-fixing *C. fairchildiana* before and during drought, and in *P. auritum* during drought. In the following discussion, we evaluate the species-specific physiological responses to drought in relation to different processes driving daytime CO_2-production and discuss metabolic implications for isoprenoid

biosynthesis in *C. fairchildiana* arising from its unique pyruvate utilization. Subsequently, we focus on the differences in biosynthesis of isoprene and monoterpenes in *C. fairchildiana* and discuss potential ramifications for biosynthetic pathways involved, including metabolic crosstalk between MVA and MEP pathways.

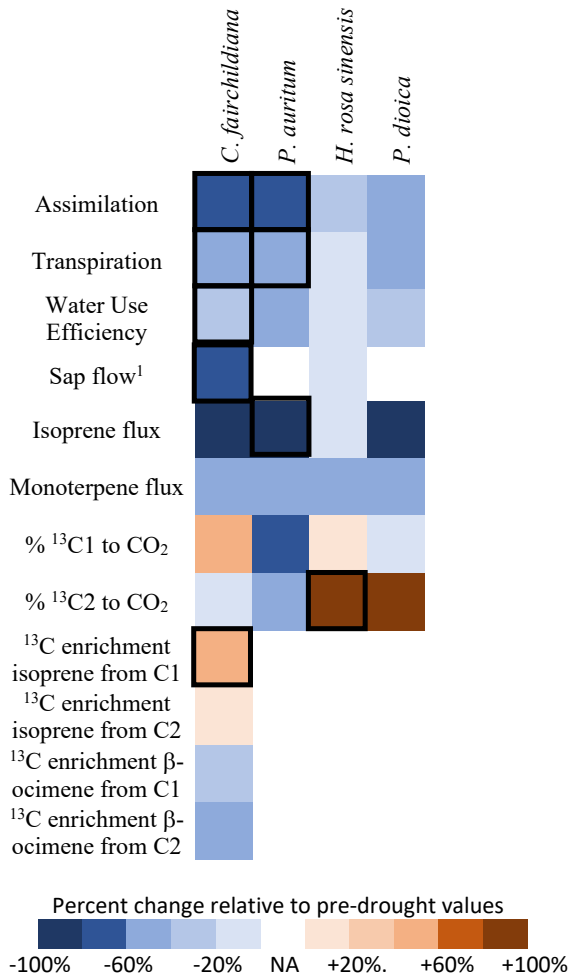

Figure 7: Trends in response to drought by *C. fairchildiana*, *P. auritum*, *H. rosa sinensis*, and *P. dioica*, expressed as percent decrease (blue shades) or increase (brown shades) of the mean drought value relative to the mean pre-drought value. Black borders indicate measurements where the mean values were significantly different at the $p < 0.05$ level. [1]Data from Werner *et al.*, 2021.

Daytime CO_2 production and relationship to drought status

Among the four species we studied, gas exchange from *H. rosa sinensis* was least affected by drought, with leaf level assimilation and transpiration rates remaining relatively consistent (**Figures 2, 7**). These rates were quite low both before and during drought, and these understory shrubs may have been light limited throughout the entire time period. *H. rosa sinensis* displayed the expected pattern of ^{13}C enrichment of CO_2 when supplied with position-specific ^{13}C-pyruvate: ^{13}C from the C1 position of pyruvate was rapidly respired, while the C2 position was not (**Figures 4, 5**) (Priault *et al.*, 2009; Werner *et al.*, 2009). This

indicates an inhibited TCA cycle, but ample CO_2 production from anabolic processes. However, TCA cycle activity in the light, as evidenced by ^{13}C enrichment of CO_2 during $^{13}C2$-pyruvate labeling, increased with drought (**Figure 4**). This increased daytime TCA cycle activity could represent an early drought response by *H. rosa sinensis*, as it can be associated with elevated synthesis of amino acids such as L-glutamate (Tcherkez *et al.*, 2009). L-glutamate, produced via the TCA cycle, is a direct precursor for the osmoprotectant proline (Delauney and Verma, 1993), which accumulates in plant cells under drought (Shinozaki and Yamaguchi-Shinozaki, 1998; Farooq *et al*., 2012). In line with this hypothesis, the roots of *H. rosa sinensis* showed pronounced accumulation of osmolytes during the B2WALD drought and upregulated synthesis of γ-aminobutyric acid (GABA) (Honneker *et al*., 2022), which can stimulate accumulation of proline (Nayyar *et al*., 2014).

Even though overall assimilation and transpiration rates did not decline significantly for *P. dioica* under drought, these rates declined for all trees except for the largest individual on the south side of the Biosphere 2 rainforest (**Figure 2**). Although gas exchange rates of *P. dioica* tended to be more affected by drought than those of *H. rosa sinensis*, the two species displayed similar trends in their CO_2 emission rates. Just like *H. rosa sinensis*, *P. dioica* converted a similar percentage of ^{13}C from $^{13}C1$-pyruvate to CO_2 before and during drought, demonstrating the importance of maintaining anabolic activities that result in the release of CO_2 even as overall carbon availability tended to decline (**Figure 4**). Likewise, there was a tendency for daytime TCA cycle activity to increase, as most leaves respired more ^{13}C from $^{13}C2$-pyruvate during the drought (**Figure 4**).

In comparison with *H. rosa sinensis* and *P. dioica*, *P. auritum* was affected much more strongly after a month of drought (**Figures 2, 7**). Before drought, all three species decarboxylated similar amounts of ^{13}C from $^{13}C1$-pyruvate, but this rate declined by 56 % for *P. auritum* during the drought (**Figure 4**). This reduction in anabolic CO_2 production was independent of the decline in gas exchange rates (**Figure S1**), suggesting that reductions in overall carbon availability are not responsible for declining CO_2 production. In contrast to *P. dioica* and *H. rosa sinensis*, the proportion of respired $^{13}C2$-pyruvate tended to decline in *P. auritum*, and may have been indicative of the more severe drought stress experienced by this species (**Figures 4, 7**). These adjustments suggest a concurrent decline in daytime CO_2 production from both mitochondrial and non-mitochondrial processes, which may have been due to less metabolic activity.

C. fairchildiana displayed the strongest physiological (**Figures 2, 7**) and structural responses to the drought, shedding ~ 25 % of its leaves (Werner *et al.* 2021), an atypical

occurrence for this evergreen tree. This leaf loss, along with reduced transpiration rates at the level of individual leaves, resulted in a 76 % reduction in sap flow (Werner *et al*., 2021). However, *C. fairchildiana* was the only species in which no changes in the percent of ^{13}C1 and ^{13}C2-pyruvate converted to CO_2 were observed (**Figures 4, 7**). Although both *P. auritum* and C. *fairchildiana* decarboxylated similarly low amounts of ^{13}C1-pyruvate under drought (**Figure 4**), the low rates observed for C. *fairchildiana* are unlikely to be driven by the same underlying mechanism as in *P. auritum*, as the percentage of ^{13}C-pyruvate that was respired was unchanged from pre-drought conditions. This suggests general differences in metabolic utilization of cytosolic carbon sources by *C. fairchildiana* in comparison to the other three species.

Metabolic link between MEP and MVA pathway shapes isoprenoid metabolism in C. fairchildiana

Among the four species we studied, only *C. fairchildiana* emitted large amounts of isoprenoid VOCs (**Figure 3; Table 1**). Previous labeling studies have observed that cytosolic pyruvate is readily incorporated into MEP-derived isoprenoids, including isoprene and monoterpenes, typically with greater ^{13}C-enrichment from ^{13}C2-pyruvate than from ^{13}C1-pyruvate (Fasbender *et al*., 2018; Yáñez-Serrano *et al*., 2019; Werner *et al*., 2020). This is most likely due to the decarboxylation of pyruvate in the MEP pathway, conserving the C2 carbon from pyruvate but not the C1 carbon (**Figures 1, 8, step 4**) (Trapp and Croteau, 2001; Dudareva *et al*., 2004). However, in *C. fairchildiana*, isoprene was similarly enriched in ^{13}C whether it was labeled by ^{13}C1- or ^{13}C2-pyruvate (**Figure 6**). This suggests that instead of directly transporting cytosolic pyruvate into the plastid, it is first converted to GA-3-P, which maintains all three carbons when it enters the MEP pathway, providing a route for ^{13}C1-pyruvate to also create ^{13}C enriched isoprenoids (**Figure 1, 8, step 2**) (Ladd *et al*., 2021). This could partially explain the low ^{13}C enrichment of CO_2 respired by *C. fairchildiana* during labeling with ^{13}C1-pyruvate, as all three carbons from the pyruvate label are conserved within the GA-3-P derived isoprenoids, including non-volatile compounds that remained within the leaf. The decline in isoprene emissions under drought (**Figure 3**) and concomitant increase of ^{13}C-enrichment from ^{13}C-pyruvate (**Figure 6**) indicates that *de novo* synthesis of isoprene from primary photosynthate by *C. fairchildiana* declined under drought as the availability of primary photosynthate also declined, resulting in an increased proportion of the remaining isoprene flux being dependent on cytosolic pyruvate via GA-3-P (**Figure 8, step 2-4**) (Souza *et al*., 2018; Yáñez-Serrano *et al*., 2019).

Differing patterns of ^{13}C-label incorporation between isoprene and trans-β-ocimene (**Figure 6**) was unexpected, since both compounds are derived from IPP and its isomer dimethylallyl pyrophosphate (DMAPP) that are produced in the MEP pathway (**Figure 1, step 4**). IPP and DMAPP are also produced in the cytosolic MVA pathway, where pyruvate is incorporated only via acetyl-CoA, with its C1 position being decarboxylated (**Figure 1, step 5**). Although exchange of these isoprenoid precursors across the plastid membrane has long been suggested as metabolic crosstalk between the MEP and MVA pathways (Arigoni *et al*., 1997; Hemerlin *et al*., 2003; Hemerlin *et al*., 2012), it remains controversial due to a lack of proven IPP transporters (Rasulov *et al*., 2018; Souza *et al*., 2018). However, transporters for geranyl pyrophosphate (GPP), an intermediate between IPP and monoterpenes that can be produced in the cytosol (Bouvier *et al*., 2001; Schmidt and Gershenzon, 2007; Zulak *et al*., 2010) as well as in the plastid, have been identified (Bick and Lange, 2003; Gutensohn *et al*., 2012).

The pattern of ^{13}C enrichment in isoprenoids produced by *C. fairchildiana* during ^{13}C-pyruvate labeling in the pre-drought period would be consistent with the transport of MVA derived GPP into the plastid, where it is subsequently converted to monoterpenes that are only enriched by $^{13}C2$-pyruvate. Alternatively, the same pattern could be observed if trans-β-ocimene was synthesized as a byproduct of sesquiterpene synthesis (Davidovich-Rikanati *et al.* 2008; Gutensohn *et al.* 2013) or via enzymes of the Nudix hydrolase family (Magnard *et al.*, 2015; Liu *et al.*, 2018) in the cytosol. However, these processes are unlikely to drive the observed patterns as *C. fairchildiana* did not emit any sesquiterpenes and the presence of monoterpene synthesis via Nudix hydrolases in vegetative tissue has yet to be shown. Therefore, the most likely explanation for the observed pattern of ^{13}C enrichment of trans-β-ocimene by $^{13}C2$-pyruvate most likely includes synthesis via MVA derived GPP as well as synthesis within the MEP pathway. Isoprene, which is not synthesized from GPP, on the other hand, is ^{13}C enriched at similar rates by both pyruvate labels since it is only sourced from MEP derived IPP/DMAPP.

During drought, trans-β-ocimene synthesis from MVA derived GPP apparently declined or even completely ceased (**Figure 8, step 5**), as the ^{13}C-enrichment of β-ocimene was similar from both $^{13}C1$- and $^{13}C2$-pyruvate, similar to isoprene (**Figure 6**). In contrast to isoprene, ^{13}C enrichment of trans-β-ocimene declined with drought, indicating less *de novo* synthesis of these compounds, even as *de novo* synthesis apparently became more important for supporting the isoprene flux (**Figure 6**). The enhanced trans-β-ocimene emissions under

drought (**Table 1**) thus may have been increasingly derived from stored intermediates (Lerdau *et al*., 1995, 1997; Niinemets *et al*., 2002), diluting the ^{13}C enrichment of trans-β-ocimene during labeling.

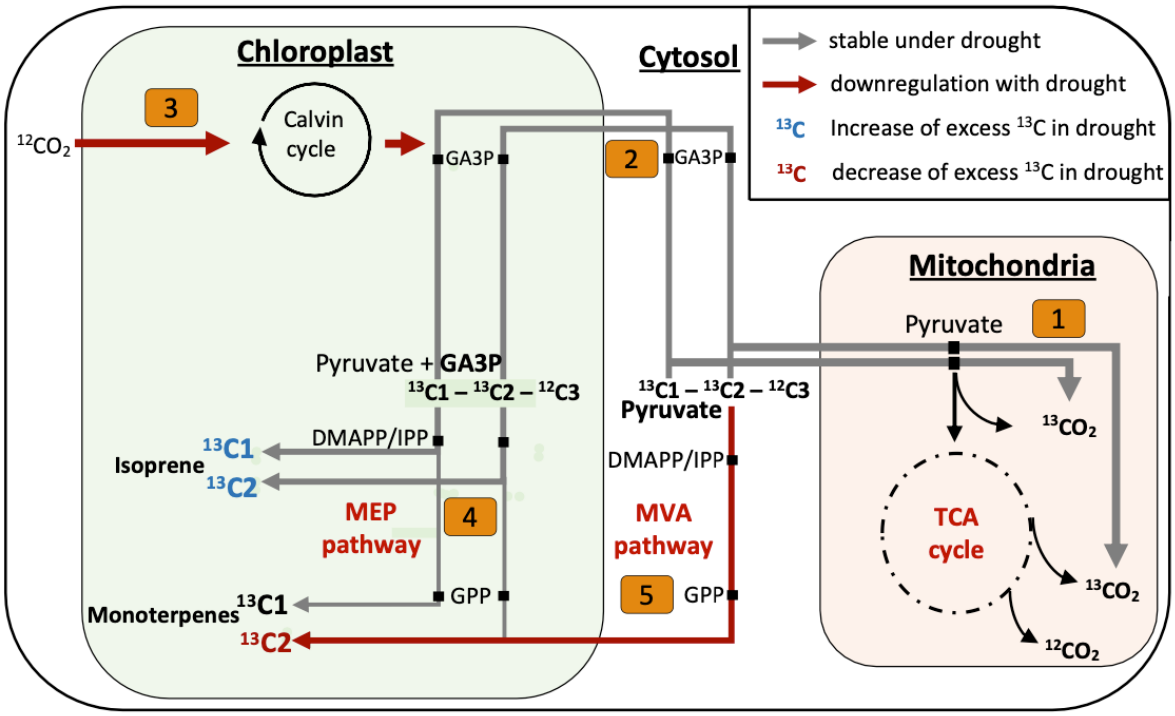

Figure 8: Schematic representation of pyruvate carbon partitioning among biosynthetic processes involved in the synthesis of isoprenoids and production of CO_2 within *Clitoria fairchildiana* cells as well as proposed adjustments of these processes during drought. Several intermediate steps and involved enzymes are removed for clarity. Arrow thickness represents the relative amount of $^{13}C1$-/ $^{13}C2$-labeled pyruvate utilized for the indicated pathway during pre-drought conditions. Gray arrows indicate no changes in carbon utilization during drought while brown arrows indicate a down-regulation of the pathway. Blue colored $^{13}C1/^{13}C2$ indicate an increase in excess ^{13}C emissions of isoprene or monoterpenes during drought, while red color indicates a decline in excess ^{13}C emissions. Numbers represent the relevant pathways discussed, with descriptions of pathways 1-5 described in the caption of Figure 1. TCA, tricarboxillic acid; GA-3-P, glyceraldehyde 3-phosphate; DMAPP Dimethylallyl pyrophosphate; IPP, isopentenyl pyrophosphate; MEP, methylerythritol phosphate; GPP, geranyl pyrophosphate; MVA, mevalonic acid.

Conclusions

We investigated leaf level metabolic effects of drought by using position specific ^{13}C-pyruvate labels to track daytime CO_2 production and isoprenoid synthesis by four tropical species before and during an experimental drought in the Biosphere 2 rainforest. Our results indicate that although the TCA cycle is inhibited during the day, daytime CO_2 production from anabolic processes can result in a substantial CO_2 flux. This carbon flux tended to decline with drought stress, perhaps due to lower availability of pyruvate from reduced

assimilation, but also from reduced allocation of the pyruvate to anabolic processes, as in the case for *P. auritum*. Meanwhile, the contribution of the TCA cycle to daytime CO_2 production, as evidenced by the relative amount of $^{13}CO_2$ produced from ^{13}C2-pyruvate, tended to increase under drought.

We also observed large reductions in isoprene emissions by *C. fairchildiana* under drought, which is likely at least partially due to lower substrate availability from lower photosynthetic activity. Additionally, the different patterns of label incorporation into isoprene and trans-β-ocimene illustrates linkages between the two pathways for isoprenoid biosynthesis, and adds to a growing body of evidence that GPP transport across the plastid membrane is more important than IPP transport for providing metabolic flexibility in isoprenoid production (Bick and Lange, 2003; Gutensohn *et al*., 2012; Ladd *et al*., 2021). Overall, our results demonstrate that metabolic plasticity in response to drought can affect daytime CO_2 production and isoprenoid synthesis.

Acknowledgements: This research was funded by the European Research Council (ERC consolidator grant 647008 to CW) and financial support from the Philecology Foundation to Biosphere 2 (obtained by LKM). The study took place within the context of the B2WALD campaign, and was supported by the wider efforts of the entire B2WALD team, as described on the team contribution list (https://doi.org/10.25422/azu.data.14632662). We are particularly grateful to Michael Burman, Marissa Clover, Sydney Kerman, and Luke Miller for their assistance with leaf labeling in the forest canopy. The authors declare no conflicts of interest.

Author Contributions: Conceptualization (CW, SNL, LED); Data curation (LED, IB, JVH, LKM), Formal analysis (LED, SNL, JK, IB, AK, JVH, GP); Funding acquisition (CW, LKM); Investigation (SNL, LED, IB, JD, JVH, GP, JI, CW, AK); Methodology (CW, JK, IB, LED, SNL); Project administration (CW, SNL); Resources (CW, JVH, LKM); Supervision (CW, LKM, SNL); Validation (AK, CW, IB, LED, SNL); Visualization (LED, SNL); Writing – original draft (SNL, LED); Writing – review & editing: all.

References:

Anjum SA, Xie XY, Wang LC, Saleem MF, Man C, Lei W. 2011. Morphological, physiological and biochemical responses of plants to drought stress. African Journal of Agricultural Research 6, 2026-2032.

Arigoni D, Sagner S, Latzel C, Eisenreich W, Bacher A, Zenk MH. 1997. Terpenoid biosynthesis from 1-deoxy-D-xylulose in higher plants by intramolecular skeletal rearrangement. Proceedings of the National Academy of Sciences of the United States of America 94, 10600-10605.

Atkin OK, Millar AH, Gardeström P, Day DA. 2000. Photosynthesis, carbohydrate metabolism and respiration in leaves of higher plants. In: Leegood RC, Sharkey TD, von Caemmerer S, eds. Photosynthesis. Photosynthesis and Respiration, vol. 9. Dordrecht: Springer, 153-175.

Bhargava S, Sawant K. 2013. Drought stress adaptation: metabolic adjustment and regulation of gene expression. Plant Breeding 132, 21-32.

Bick JA, Lange BM. 2003. Metabolic cross talk between cytosolic and plastidial pathways of isoprenoid biosynthesis: unidirectional transport of intermediates across the chloroplast envelope membrane. Archives of Biochemistry and Biophysics 415, 146-154.

Bouvier F, Suire C, D'Harlingue A, Backhaus RA, Camara B. 2001. Molecular cloning of geranyl diphosphate synthase and compartmentation of monoterpene synthesis in plant cells. The Plant Journal 24, 241-252.

Davidovich-Rikanati R, Lewinsohn E, Bar E, Iijima Y, Picherksy E, Sitrit Y. 2008. Overexpression of the lemon basil α-zingiberene synthase gene increases both mono- and sesquiterpene contents in tomato fruit. The Plant Journal 56, 228-238.

Delauney AJ, Verma DPS. 1993. Proline biosynthesis and osmoregulation in plants. The Plant Journal 4, 215-223.

Dudareva N, Pichersky E, Gershenzon J. 2004. Biochemistry of plant volatiles. Plant Physiology 135, 1893-1902.

Dudareva N, Negre F, Nagegowda DA, Orlova I. 2006. Plant volatiles: recent advances and future perspectives. Critical Reviews in Plant Sciences 25, 417-440.

Farooq M, Hussain M, Wahid A, Siddique KHM. 2012. Drought stress in plants: An Overview. In: Aroca R, ed. Plant responses to drought stress. Berlin: Springer, 1-33.

Fasbender L, Yáñez-Serrano AM, Kreuzwieser J, Dubbert D, Werner, C. 2018. Real-time carbon allocation into biogenic volatile organic compounds (BVOCs) and respiratory carbon dioxide (CO_2) traced by PTR-TOF-MS, $^{13}CO_2$ laser spectroscopy and ^{13}C-pyruvate labelling. PLOS One 13, e0204398.

Ghirardo A, Gutknecht J, Zimmer I, Brüggemann N, Schnitzler J-P. 2011. Biogenic volatile organic compound and respiratory CO_2 emissions after ^{13}C-labeling: online tracing of C translocation dynamics in poplar plants. PloS One 6, e17393.

Guenther A, Hewitt CN, Erickson D, *et al*. 1995. A global model of natural volatile organic compound emissions. Journal of Geophysical Research: Atmospheres 100, 8873-8892.

Gutensohn M, Nagegowda DN, Dudareva N. 2012. Involvement of compartmentalization in monoterpene and sesquiterpene biosynthesis in plants. In: Bach TJ, Rohmer M, eds. Isoprenoid Synthesis in Plants and Microorganisms. New York: Springer Science and Business Media, 155-169.

Gutensohn M, Orlova I, Nguyen TTH, Davidovich-Rikanati R, Ferruzzi MG, Sitrit Y, Lewinsohn E, Pichersky E, Dudareva N. 2013. Cytosolic moterpene biosynthesis is supported by plastid-generated geranyl diphosphate substrate in transgenic tomato fruits. The Plant Journal 75, 351-363.

Haberstroh S, Kreuzwieser J, Lobo-do-Vale R, Caldeira MC, Werner C. 2018. Terpenoid emissions of two Mediterranean woody species in response to drought stress. Frontiers in Plant Science 9, 1071. doi: 10.3389/fpls.2018.01071

Harrison SP, Morfopoulos C, Srikanta Dani KG, *et al*. 2013. Volatile isoprenoid emissions from plastid to planet. New Phytologist 197, 49-57.

Hayes JM. 2004. An introduction to isotopic calculations. Woods Hole Oceanographic Institution, Woods Hole, MA, 2543.

Hemmerlin A, Hoeffler J-F, Meyer O, Tritsch D, Kagan IA, Grosdemange-Billiard C, Rohmer M, Bach TJ. 2003. Crosstalk between the cytosolic mevalonate and the plastidial methylerythritol phosphate pathways in tobacco bright yellow-2 cells. Journal of Biological Chemistry 278, 26666-26676.

Hemmerlin A, Harwood JL, Bach, TJ. 2012. A *raison d'être* for two distinct pathwys in the early steps of plant isoprenoid biosynthesis? Progress in Lipid Research 5, 95-148.

Heskel MA, Atkin OK, Turnbull MH, Griffin KL. 2013. Bringing the Kok effect to light: a review on the integration of daytime respiration and net ecosystem exchange. Ecosphere 4, 1-14.

Honeker L, Hildebrand G, Fudyma J, *et al*. 2021. Elucidating drought tolerance mechanisms in plant roots through 1H-NMR metabolomics, MALDI-MS, and NanoSIMS imaging technologies. Environmental Science & Technology 56, 2021-2032.

Hubau W, Lewis SL, Phillips OL, *et al.* 2020. Asynchronous carbon sink saturation in African and Amazonian tropical forests. Nature 579, 80-87.

Jardine K, Wegener F, Abrell L, van Haren J, Werner C. 2014. Phytogenic biosynthesis and emission of methyl acetate. Plant, Cell & Environment 37, 414–424.

Ladd SN, Nelson DB, Bamberger I, Daber LE, Kreuzwieser J, Kahmen A, Werner C. 2021. Metabolic exchange between pathways for isoprenoid synthesis and implications for biosynthetic hydrogen isotope fractionation. New Phytologist 231, 1708-1719.

Lerdau M, Matson P, Fall R, Monson R. 1995. Ecological controls over monoterpene emissions from Douglas fir (*Pseudotsuga menziesii*). Ecology 76, 2640-2647.

Lerdau M, Guenther A, Monson R. 1997. Plant production and emission of volatile organic compounds. BioScience 47 6, 373-383.

Lichtenthaler HK, Rohmer M, Schwender J. 1997. Two independent biochemical pathways for isopentenyl diphosphate and isoprenoid biosynthesis in higher plants. Physiologia Plantarum 101, 643-652.

Liu J, Guan Z, Liu H, Qi L, Zhang D, Zou T, Yin P. 2018. Structural insights into the substrate recognition mechanism of *Arabidopsis* GPP-bound NUDX1 for noncanonical monoterpene biosynthesis. Molecular Plant 11, 218-221.

Magnard J-L, Roccia A, Caissard J-C, Vergne P, Sun P, Hecquet R, Dubois A, Oyant L H-S, Jullien F, Nicole F, Raymond O, Huguet S, Baltenweck R, Meyer S, Claudel P, Jeauffre J, Rohmer M, Foucher F, Hugueney P, Bendahmane M, Baudino S. 2015. Biosynthesis of monoterpene scent compounds in roses. Science 349, 81-83.

Massé G, Belt ST, Rowland SJ, Rohmer M. 2004. Isoprenoid biosynthesis in the diatoms *Rhizolenia setigera* (Brightwell) and *Haslea ostrearia* (Simonsen). Proceedings of the National Academy of Sciences of the United States of America 101, 4413-4418.

Materić D, Bruhn D, Turner C, Morgan G, Mason N, Gauci V. 2015. Methods in plant foliar volatile organic compounds research. Applications in Plant Sciences 3, 1500044.

Metcalfe DB, Meir P, Aragao LEOC, Lobo-do-Vale R, *et al.* 2010. Shifts in plant respiration and carbon use efficiency at a large-scale drought experiment in the eastern Amazon. New Phytologist 187, 608-621.

Mitchard ETA. 2018. The tropical forest carbon cycle and climate change. Nature 559, 537-534.

Monson RK, Fall R. 1989. Isoprene emissions from aspen leaves: influence of environment and relation to photosynthesis and photorespiration. Plant physiology 90, 267-74.

Nayyar H, Kaur R, Kaur S, Singh R. 2014. γ-Aminobutyric acid (GABA) imparts partial protection from heat stress injury to rice seedlings by improving leaf turgor and upregulating osmoprotectants and antioxidants. Journal of Plant Growth Regulation 33, 408-419.

Niinemets Ü, Reichstein M. (2002). A model analysis of the effects of nonspecific monoterpenoid storage in leaf tissues on emission kinetics and composition in Mediterranean sclerophyllous Quercus species. Global Biogeochemical Cycles 16, 57–1.

Niinemets, Ü. 2010. Mild versus severe stress and BVOCs: thresholds, priming and consequences. Trends in Plant Science 15, 145–153.

O'Leary BM, Asao S, Miller AH, Atkin OK. 2019. Core principles which explain variation in respiration across biological scales. New Phytologist 222, 670-686.

Peñuelas J, Staudt M. 2010. BVOCs and global change. Trends in Plant Science 15, 133-144.

Pinheiro C, Chaves MM. 2011. Photosynthesis and drought: can we make metabolic connections from available data? Journal of experimental botany 62, 869-882.

Priault P, Wegener F, Werner C. 2009. Pronounced differences in diurnal variation of carbon isotope composition of leaf respired CO_2 among functional groups. New Phytologist, 181, 400-412.

Rascher U, Bobich EG, Lin GH, *et al.* 2004. Functional diversity of photosynthesis during drought in a model tropical rainforest - the contributions of leaf area, photosynthetic electron transport and stomatal conductance to reduction in net ecosystem carbon exchange. Plant, Cell & Environment 27, 1239-1256.

Rasmussen RA. 1970. Isoprene: Identified as a forest-type emission in the atmosphere. Environmental Science and Technology 4, 667-671.

Rasulov B, Talts E, Bichele I, Niinemets Ü. 2018. Evidence that isoprene emission is not limited by cytosolic metabolites. Exogenous malate does not invert the reverse sensitivity of isoprene emission to high [CO_2]. Plant Physiology 176, 1573-1586.

Reddy AR, Chaitanya KV, Vivekanandan M. 2004. Drought-induced responses of photosynthesis and antioxidant metabolism in higher plants. Journal of Plant Physiology 161, 1189-1202.

Rosolem R, Shuttleworth WJ, Zeng X, Saleska SR, Huxman TE. 2010. Land surface modeling inside the Biosphere 2 tropical rain forest biome. Journal of Geophysical Research Atmospheres 115, doi: 10.1029/2010JG001443

Schimel D, Pavlick R, Fisher JB, Asner GP, Saatchi S, Townsend P, Miller C, Frankenberg C, Hibbard K, Cox P. 2015. Observing terrestrial ecosystems and the carbon cycle from space. Global Change Biology 21, 1762-1776.

Schmitt A, Gershenzon J. 2007. Cloning and characterization of isoprenyl diphosphate synthases with farnesyl diphosphate and geranylgeranyl diphosphate synthase activity from Norway spruce (*Picea abies*) and their relation to induced oleoresin formation. Phytochemistry 68, 2649-2659.

Schuhr CA, Radykewicz T, Sagner S, Latzel C, Zenk MH, Arigoni D, Bacher A, Rohdich F, Eisenreich W. 2003. Quantitative assessment of crosstalk between the two isoprenoid biosynthesis pathways in plants by NMR spectroscopy. Phytochemistry Reviews 2, 3-16

Schwender J, Seemann M, Lichtenthaler HK, Rohmer M. 1996. Biosynthesis of isoprenoids (carotenoids, sterols, prenyl side-chains of chlorophylls and plastoquinone) via a novel pyruvate/glyceraldehyde 3-phosphate non-mevalonate pathway in the green alga *Scenedesmus obliquus*. Biochemistry Journal 316, 73-80.

Shinozaki K, Yamaguchi-Shinozaki K. 1998. Molecular responses to drought stress. In: Satoh K, Murata N, (eds). Stress responses of photosynthetic organisms. Amsterdam: Elsevier Science, 149-163

Souza VF, Niinemets Ü, Rasulov B, Vickers CE, Duvoisin Júnior S, Araújo WL. Concalves JFC. 2018. Alternative carbon sources for isoprene emission. Trends in Plant Science 23, 1081-1101.

Sweetlove LJ, Williams TCR, Maurice Cheung CY, Ratcliffe RG. 2013. Modelling metabolic CO_2 evolution – a fresh perspective on respiration. Plant, Cell & Environment 36, 1631-1640.

Tcherkez G, Cornic G, Bligny R, Gout E, Ghashghaie J. 2005. In vivo respiratory metabolism of illuminated leaves. Plant Physiology 138, 1596-1606.

Tcherkez G, Bligny R, Gout E, Mahé A, Hodges M, Cornic G. 2008. Respiratory metabolism of illuminated leaves de- pends on CO2 and O2 conditions. Proceedings of the National Academy of Sciences of the United States of America 105, 797–802.

Tcherkez G, Mahé A, Cauthier P, Mauve C, Gout E, Bligny R, Cornic G, Hodges M. 2009. In folio respiratory fluxomics revealed by ^{13}C isotopic labeling and H/D isotope effects highlight the noncyclic nature of the the tricarboxylic acid "cycle" in illuminated leaves. Plant Physiology 151, 620-630.

Tcherkez G, Boex-Fontvieille E, Mahé A, Hodges M. 2012. Respiratory carbon fluxes in leaves. Current Opinion in Plant Biology 15 308-314.

Tcherkez G, Gauthier P, Buckley TN, *et al.* 2017. Leaf day respiration: low CO 2 flux but high significance for metabolism and carbon balance. New Phytologist 216, 986-1001.

Trapp S, Croteau R. 2001. Defensive resin biosynthesis in conifers. Annual Review of Plant Biology 52, 689-724.

von Caemmerer S, Farquhar GD. 1981. Some relationships between the biochemistry of photosynthesis and the gas exchange of leaves. Planta 153, 376-387.

Wehr R, Munger JW, McManus JB, Nelson DD, Zahniser MS, Davidson EA, Wofsy SC, Saleska SR. 2016. Seasonality of temperate forest photosynthesis and daytime respiration. Nature 534, 680-683.

Wegener F, Beyschlag W, Werner C. 2010. The magnitude of diurnal variation in carbon isotopic composition of leaf dark respired CO_2 correlates with the difference between $\delta^{13}C$ of leaf and root material. Functional Plant Biology 37, 849-858.

Werner C, Wegener F, Unger S, Nogués S, Priault P. 2009. Short-term dynamics of isotopic composition of leaf respired CO_2 upon darkening: measurements and implications. Rapid Communications in Mass Spectrometry 23, 2428–2438.

Werner C, Fasbender L, Romek KM, Yáñez-Serrano AM, Kreuzwieser, J. 2020. Heat waves change plant carbon allocation among primary and secondary metabolism altering CO_2 assimilation, respiration, and VOC emissions. Frontiers in Plant Science 11, 1242.

Werner C, Meredith LK, Ladd SN, *et al.* 2021. Ecosystem fluxes during drought and recovery in an experimental forest. Science 374, 1514-1518.

Yáñez-Serrano AM, Mahlau L, Fasbender L, Byron J, Williams J, Kreuzwieser J, Werner C. 2019. Heat stress increases the use of cytosolic pyruvate for isoprene biosynthesis. Journal of Experimental Botany 70, 5827-5838.

Zhao J, Hartmann H, Trumbore S, Ziegler W, Zhang Y. 2013. High temperature causes negative whole-plant carbon balance under mild drought. New Phytologist 200, 330-339.

Zulak KG, Bohlmann, J. 2010. Terpenoid biosynthesis and specialized vascular cells of conifer defense. Journal of Integrative Plant Biology 52, 86-97

Tables:

Table 1: Fluxes of common monoterpenes emitted by *Clitoria fairchildiana*, as determined by GC-MS analysis. Monoterpene fluxes from the other three species were too low for quantification by GC-MS. Fluxes are reported as mean and standard error. [1]These two compounds co-eluted on the GC and the combined flux is reported.

	Pre-drought flux (pmol m^{-2} s^{-1})		Drought flux (pmol m^{-2} s^{-1})		Significant change with drought
α-pinene	6.51	± 2.41	3.09	± 0.20	$p < 0.001$
d-3-carene/ β-pinene[1]	9.28	± 2.96	5.52	± 0.46	$p < 0.01$
limonene	5.10	± 0.79	4.39	± 0.23	$p < 0.05$
trans-β-ocimene	5.47	± 1.20	28.88	± 7.35	$p < 0.0001$

Figure captions:

Figure 1: Schematic representation of important processes for the synthesis of isoprenoids and production of CO_2 within plant cells, with several intermediate steps removed for clarity. Green arrows represent possible movement of carbon from the C1 position of pyruvate and purple arrows represent movement of carbon from the C2 position of pyruvate. Numbers represent the relevant pathways discussed. 1: Transport of pyruvate into mitochondria, followed by initial decarboxylation of the C1-position and entrance into the TCA-cycle. 2: Conversion of pyruvate to GA-3-P and transport into the chloroplast. Pyruvate might also be transported directly to the chloroplast. All carbon positions of pyruvate remain in both cases. 3: Entrance of CO_2 into the Calvin cycle and addition of GA-3-P and other assimilation products into the metabolic pool of the chloroplast. 4: Initial reaction of pyruvate and GA-3-P to form DMAPP and IPP via MEP pathway, followed by reaction of two DMAPP/IPP molecules to produce GPP. As GA-3-P is not decarboxylated in this reaction, all carbon positions of the converted GA-3-P remain in the produced isoprene and monoterpenes. Pyruvate on the other hand is decarboxylated, resulting in only the C2-position remaining in these products 5: Entrance of pyruvate into MVA pathway and initial decarboxylation of the C1-position of pyruvate to form DMAPP, IPP and subsequently GPP in the cytosol. After transport of these metabolites incorporating the ^{13}C2-label into the chloroplast, DMAPP and IPP can either enter isoprene or monoterpene synthesis, while GPP is utilized to synthesize monoterpenes. TCA, tricarboxlic acid; GA-3-P, glyceraldehyde 3-phosphate; DMAPP Dimethylallyl pyrophosphate; IPP, isopentenyl pyrophosphate; MEP, methylerythritol phosphate; GPP, geranyl pyrophosphate; MVA, mevalonic acid.

Figure 2: Representative leaves (panel a) and rates of (b) carbon assimilation, (c) transpiration, and (d) instantaneous water use efficiency measured on individual leaves of *Clitoria fairchildiana*, *Piper auritum, Hibiscus rosa sinensis*, and *Phytolacca dioica* under pre-drought (green) and drought (brown) conditions. Boxes represent the median and 25 – 75 % range of 7-12 replicate leaves. Whiskers and outliers calculated using Tukey's method. Significant differences between pre-drought and drought conditions for each species are indicated as * when $p < 0.05$, ** when $p < 0.01$, and *** when $p < 0.001$.

Figure 3: Emission rates of (a) isoprene and (b) monoterpenes measured on individual leaves of *Clitoria fairchildiana*, *Piper auritum, Hibiscus rosa sinensis*, and *Phytolacca dioica* under pre-drought (green) and drought (brown) conditions. Fluxes from *C. fairchildiana* are plotted on the left y-axis while all other species are plotted on the right y-axis. Boxes represent the median and 25 – 75 % range of 7-12 replicate leaves. Whiskers and outliers are calculated using Tukey's method. Significant differences between pre-drought and drought conditions for each species are indicated as: * when $p < 0.05$.

Figure 4 Percent of ^{13}C from ^{13}C1-labeled pyruvate (left column) and ^{13}C2-labeled pyruvate (right column) that was released as CO_2 by *Clitoria fairchildiana*, *Piper auritum, Hibiscus rosa sinensis*, and *Phytolacca dioica* under pre-drought (panel a) and drought (panel b)

conditions. Boxes represent the median and 25 – 75 % range of 3 - 6 replicate leaves. Whiskers and outliers are calculated using Tukey's method. Significant differences among groups as determined by three-way ANOVA with Tukey's posthoc test are indicated as: * when $p < 0.05$, ** when $p < 0.01$, *** when $p < 0.001$, and **** when $p < 0.0001$.

Figure 5 ^{13}C enrichment of CO_2 from $^{13}C1$-labeled pyruvate (y-axis) plotted relative to ^{13}C enrichment of CO_2 from $^{13}C2$-labeled pyruvate (x-axis) during pre-drought (open symbols) and drought (closed symbols). Symbols represent mean values and error bars represent one standard deviation of 3 – 6 replicate leaves per species.

Figure 6: ^{13}C from ^{13}C-labeled pyruvate incorporation into VOCs from *Clitoria fairchildiana*. (a) ^{13}C excess isoprene emissions relative to natural background ^{13}C abundance for isoprene and (b) ^{13}C enrichment of the monoterpene trans-β-ocimene relative to unlabeled measurements during pre-drought (green) and drought (brown) (4 – 6 replicates per treatment). Boxes represent median and 25-75% range of 7-12 replicate leaves. Whiskers and outliers are calculated using Tukey's method.

Figure 7: Trends in response to drought by *C. fairchildiana*, *P. auritum*, *H. rosa sinensis*, and *P. dioica*, expressed as percent decrease (blue shades) or increase (brown shades) of the mean drought value relative to the mean pre-drought value. Black borders indicate measurements where the mean values were significantly different at the $p < 0.05$ level. [1]Data from Werner *et al*., 2021.

Figure 8: Schematic representation of pyruvate carbon partitioning among biosynthetic processes involved in the synthesis of isoprenoids and production of CO_2 within *Clitoria fairchildiana* cells as well as proposed adjustments of these processes during drought. Several intermediate steps and involved enzymes are removed for clarity. Arrow thickness represents the relative amount of $^{13}C1$-/ $^{13}C2$-labeled pyruvate utilized for the indicated pathway during pre-drought conditions. Gray arrows indicate no changes in carbon utilization during drought while brown arrows indicate a down-regulation of the pathway. Blue colored $^{13}C1/^{13}C2$ indicate an increase in excess ^{13}C emissions of isoprene or monoterpenes during drought, while red color indicates a decline in excess ^{13}C emissions. Numbers represent the relevant pathways discussed, with descriptions of pathways 1-5 described in the caption of Figure 1. TCA, tricarboxillic acid; GA-3-P, glyceraldehyde 3-phosphate; DMAPP Dimethylallyl pyrophosphate; IPP, isopentenyl pyrophosphate; MEP, methylerythritol phosphate; GPP, geranyl pyrophosphate; MVA, mevalonic acid.